



Search for Low-Mass Weakly Interacting Massive Particles with SuperCDMS

R. Agnese,¹⁸ A. J. Anderson,^{4,*} M. Asai,⁸ D. Balakishiyeva,¹⁸ R. Basu Thakur,^{2,19} D. A. Bauer,² J. Beaty,²⁰ J. Billard,⁴ A. Borgland,⁸ M. A. Bowles,¹¹ D. Brandt,⁸ P. L. Brink,⁸ R. Bunker,¹¹ B. Cabrera,¹⁰ D. O. Caldwell,¹⁵ D. G. Cerdeno,¹³ H. Chagani,²⁰ Y. Chen,¹¹ M. Cherry,⁸ J. Cooley,⁹ B. Cornell,¹ C. H. Crewdson,⁶ P. Cushman,²⁰ M. Daal,¹⁴ D. DeVaney,²⁰ P. C. F. Di Stefano,⁶ E. Do Couto E Silva,⁸ T. Doughty,¹⁴ L. Esteban,¹³ S. Fallows,²⁰ E. Figueroa-Feliciano,⁴ G. L. Godfrey,⁸ S. R. Golwala,¹ J. Hall,⁵ S. Hansen,² H. R. Harris,¹² S. A. Hertel,⁴ B. A. Hines,¹⁶ T. Hofer,²⁰ D. Holmgren,² L. Hsu,² M. E. Huber,¹⁶ A. Jastram,¹² O. Kamaev,⁶ B. Kara,⁹ M. H. Kelsey,⁸ S. Kenany,¹⁴ A. Kennedy,²⁰ M. Kiveni,¹¹ K. Koch,²⁰ A. Leder,⁴ B. Loer,² E. Lopez Asamar,¹³ R. Mahapatra,¹² V. Mandic,²⁰ C. Martinez,⁶ K. A. McCarthy,⁴ N. Mirabolfathi,¹⁴ R. A. Moffatt,¹⁰ R. H. Nelson,¹ L. Novak,¹⁰ K. Page,⁶ R. Partridge,⁸ M. Pepin,²⁰ A. Phipps,¹⁴ M. Platt,¹² K. Prasad,¹² M. Pyle,¹⁴ H. Qiu,⁹ W. Rau,⁶ P. Redl,¹⁰ A. Reisetter,¹⁷ R. W. Resch,⁸ Y. Ricci,⁶ M. Ruschman,² T. Saab,¹⁸ B. Sadoulet,^{14,3} J. Sander,²¹ R. L. Schmitt,² K. Schneck,⁸ R. W. Schnee,¹¹ S. Scorza,⁹ D. N. Seitz,¹⁴ B. Serfass,¹⁴ B. Shank,¹⁰ D. Speller,¹⁴ A. Tomoda,⁸ S. Upadhyayula,¹² A. N. Villano,²⁰ B. Welliver,¹⁸ D. H. Wright,⁸ S. Yellin,¹⁰ J. J. Yen,¹⁰ B. A. Young,⁷ and J. Zhang²⁰

(SuperCDMS Collaboration)

¹Division of Physics, Mathematics, & Astronomy, California Institute of Technology, Pasadena, California 91125, USA

²Fermi National Accelerator Laboratory, Batavia, Illinois 60510, USA

³Lawrence Berkeley National Laboratory, Berkeley, California 94720, USA

⁴Department of Physics, Massachusetts Institute of Technology, Cambridge, Massachusetts 02139, USA

⁵Pacific Northwest National Laboratory, Richland, Washington 99352, USA

⁶Department of Physics, Queen's University, Kingston, Ontario K7L 3N6, Canada

⁷Department of Physics, Santa Clara University, Santa Clara, California 95053, USA

⁸SLAC National Accelerator Laboratory/Kavli Institute for Particle Astrophysics and Cosmology,
2575 Sand Hill Road, Menlo Park, California 94025, USA

⁹Department of Physics, Southern Methodist University, Dallas, Texas 75275, USA

¹⁰Department of Physics, Stanford University, Stanford, California 94305, USA

¹¹Department of Physics, Syracuse University, Syracuse, New York 13244, USA

¹²Department of Physics, Texas A&M University, College Station, Texas 77843, USA

¹³Departamento de Física Teórica and Instituto de Física Teórica UAM/CSIC,
Universidad Autónoma de Madrid, 28049 Madrid, Spain

¹⁴Department of Physics, University of California, Berkeley, California 94720, USA

¹⁵Department of Physics, University of California, Santa Barbara, California 93106, USA

¹⁶Department of Physics, University of Colorado Denver, Denver, Colorado 80217, USA

¹⁷Department of Physics, University of Evansville, Evansville, Indiana 47722, USA

¹⁸Department of Physics, University of Florida, Gainesville, Florida 32611, USA

¹⁹Department of Physics, University of Illinois at Urbana-Champaign, Urbana, Illinois 61801, USA

²⁰School of Physics and Astronomy, University of Minnesota, Minneapolis, Minnesota 55455, USA

²¹Department of Physics, University of South Dakota, Vermillion, South Dakota 57069, USA

(Received 12 March 2014; revised manuscript received 6 May 2014; published 20 June 2014)

We report a first search for weakly interacting massive particles (WIMPs) using the background rejection capabilities of SuperCDMS. An exposure of 577 kg days was analyzed for WIMPs with mass $< 30 \text{ GeV}/c^2$, with the signal region blinded. Eleven events were observed after unblinding. We set an upper limit on the spin-independent WIMP-nucleon cross section of $1.2 \times 10^{-42} \text{ cm}^2$ at $8 \text{ GeV}/c^2$. This result is in tension with WIMP interpretations of recent experiments and probes new parameter space for WIMP-nucleon scattering for WIMP masses $< 6 \text{ GeV}/c^2$.

DOI: 10.1103/PhysRevLett.112.241302

PACS numbers: 95.35.+d, 29.40.Wk, 95.55.Vj

Evidence on galactic and cosmological scales strongly indicates that $\sim 80\%$ of the matter density of the Universe consists of nonluminous, nonbaryonic dark matter, whose particle nature remains unknown [1]. Weakly interacting

massive particles (WIMPs) are one class of theoretically well-motivated candidates for dark matter and may be detectable by searching for keV-scale nuclear recoils in terrestrial detectors [2]. Recent excesses of events reported

by CDMS II (Si) [3], CoGeNT [4], CRESST-II [5], DAMA [6], and possible indirect evidence from gamma rays from the galactic center [7] may have been caused by a light WIMP with mass in the $6\text{--}30\text{ GeV}/c^2$ range. A variety of theoretical models also favor light WIMPs in this mass range [8–15].

Since light WIMPs produce only low-energy nuclear recoils, experiments optimized for masses $\gtrsim 30\text{ GeV}/c^2$ have searched for light WIMPs by lowering their analysis energy thresholds [16–19]. This additional sensitivity comes with higher background rates because resolution effects degrade particle discrimination at low energies. Following this approach, we analyzed low-energy recoils in the range of $1.6\text{--}10\text{ keV}_{\text{nr}}$ (nuclear-recoil equivalent energy) from the SuperCDMS experiment at the Soudan Underground Laboratory (SUL) [20,21]. Although background discrimination gradually degrades with decreasing event energy, some discrimination can still be achieved using the relative signals measured by the different readout channels on each detector.

SuperCDMS at Soudan is an upgrade to the Cryogenic Dark Matter Search (CDMS II) [22] with new detector hardware and is operating in the same location with the same low-radioactivity setup [23]. The target consists of 15 0.6-kg cylindrical germanium crystals stacked in groups of three to form five towers. These detectors known as iZIPs are instrumented with interleaved ionization and phonon sensors on their flat faces. From the measured ionization and phonon energy, we derive the recoil energy and the “ionization yield,” the ratio between ionization and recoil energy. Nuclear recoils expected from WIMPs exhibit a reduced ionization yield compared to electron recoils, which are expected from most backgrounds. The iZIP sensor layout improves the ability to define a fiducial volume in the bulk (fiducialization) compared to the CDMS II design [24]. The fraction of the total phonon or ionization energy measured by the outer radial (guard) sensors provides radial fiducialization through the “radial partition” parameter, and the fraction measured by the sensors on each face provides fiducialization in the direction perpendicular to the flat faces through the “z partition” parameter. Such fiducialization rejects events in the peripheral regions of the detectors. These “surface events” often suffer from a reduced ionization signal, thus, polluting the WIMP signal region.

The SuperCDMS payload has been operating in SUL since March 2012. The data presented here, recorded between October 2012 and June 2013, are a subset of the ongoing exposure. The seven detectors with the lowest trigger thresholds are used for this search. The remaining detectors are used to reject events with energy deposition in more than one detector. Kolmogorov-Smirnov tests are used to remove periods of abnormal phonon behavior, poor detector neutralization, and elevated noise. The data are tested in $\sim 3\text{-}h$ units against template data sets that represent

typical periods of operation. Approximately 10% of the data are rejected by this technique, primarily due to the noise requirement. After accounting for these losses, the exposure is 577 kg days. To prevent bias when defining the event-selection criteria, all single-detector hits with recoil energies between a time-dependent noise threshold and $10\text{ keV}_{\text{nr}}$ and with ionization energy consistent with nuclear recoils were blinded. An exception was made for periods following ^{252}Cf calibrations, when background rates were higher because of the neutron activation of the detectors and their copper housings. This “open” data set constitutes 97 kg days of exposure that is distinct from the 577 kg days of data analyzed for WIMPs and was not used in the final limit calculation or to optimize the selection criteria.

For the detectors analyzed, the standard deviation of the baseline noise is $\lesssim 260\text{ eV}$ for the sum of all eight phonon channels and $\lesssim 460\text{ eV}_{\text{ee}}$ (electron-recoil equivalent) for individual ionization channels. The electron- and nuclear-recoil energy scales are calibrated in a fashion similar to the CDMS II light-WIMP search [17] using ^{133}Ba and ^{252}Cf sources, respectively. A small ($\lesssim 10\%$) variation of the phonon signal gain with the cryostat base temperature, which varied over the range of 54–62 mK, is taken into account by the phonon calibration. The measured total phonon energy is the sum of the full recoil energy of the event and Luke-Neganov phonons [25,26] produced in proportion to the ionization energy. The nuclear-recoil equivalent energy scale of each detector is set by subtracting the Luke-Neganov component corresponding to the mean ionization energy of nuclear recoils in that detector as a function of total phonon energy. These mean ionization energies, which vary slightly from detector to detector, were measured from nuclear recoils in ^{252}Cf calibration data and are generally consistent with the prediction of Lindhard [27,28]. A nuclear-recoil band was also constructed by accepting events within 3σ of the mean ionization energy.

Hardware trigger thresholds for each detector were adjusted several times during the WIMP search. For each period of constant trigger threshold, the trigger efficiencies as functions of total phonon energy were measured using ^{133}Ba calibration data. The fit results were found to be consistent with and more precise than ones obtained using ^{252}Cf and multiple-hit WIMP-search data. Analysis thresholds are set to be 1σ below the energy at which the detector trigger efficiency is 50% in periods of time for which this quantity is above the noise threshold used in the data blinding and equal to such threshold, otherwise. The combined efficiency shown in Fig. 1 is an exposure-weighted sum of the measured efficiency for each detector and period.

To be selected as WIMP candidates, the triggered events had to pass three levels of data-selection criteria: data quality, preselection, and event discrimination. Figure 1

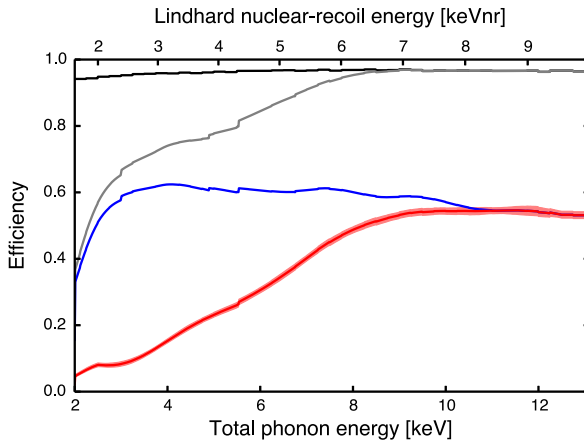


FIG. 1 (color online). Cumulative efficiencies after sequential application of each stage of event selection. From top to bottom, these are data-quality criteria, trigger and analysis thresholds, preselection criteria, and BDT discrimination with 68% C.L. (stat + syst) uncertainty band. The preselection and BDT selection efficiencies are interpolated from measurements in 1-keV bins. Steps are due to time-dependent analysis thresholds for individual detectors. For illustrative purposes, the Lindhard nuclear-recoil energy is provided as an approximate nuclear-recoil energy scale.

shows the cumulative efficiency after applying each level of selection criteria and the analysis thresholds. The first level of criteria (data quality) rejects poorly reconstructed and noise-induced events. Periods of abnormal noise are removed by requiring that the pretrigger baseline noise of each event be consistent with normal periods. Spurious triggers caused by electronic glitches and low-frequency noise in the phonon channels, which populate the low-energy region, were rejected using a pulse-shape discrimination method. Using a Monte Carlo pulse simulation that added experimental noise to template pulses to account for variation in the noise environment, the WIMP acceptance of this data-quality selection was determined to be $\gtrsim 95\%$.

The second level of event-selection criteria (preselection) removes event configurations inconsistent with WIMPs. Events coincident with the muon veto are rejected (98.7% acceptance). A single-scatter requirement removes events with energy depositions in multiple detectors, a common signature for background interactions but not expected for a WIMP-nucleon scatter ($> 99\%$ acceptance, with losses due to noise fluctuations). We also require events to lie within the 3σ nuclear-recoil band and to have phonon partitions consistent with bulk nuclear recoils. A loose fiducial volume constructed from the ionization partitions further restricts events to be consistent with bulk nuclear recoils. In the radial direction, events near the detectors' sidewalls are rejected by requiring the guard electrodes on both faces to be within 2σ from the mean of the baseline noise. For one detector (T5Z3) that has a malfunctioning guard electrode on one side, this requirement is applied on only the functioning face. A second detector (T5Z2) suffered

sporadic excess noise on one guard, so only the guard on the functioning face was used for part of the data set. These detectors were included because they increased the expected sensitivity of the analysis, especially at WIMP masses above $10 \text{ GeV}/c^2$. In the z direction, events on the flat faces are excluded by requiring that the inner electrodes on each side measure similar ionization energies [24].

The final level of event selection (discrimination) uses a boosted decision tree (BDT) [29]. The discriminators used by the BDT are the total phonon energy, ionization energy, phonon radial partition, and phonon z partition. Near threshold, the latter two variables provide identification of surface events superior to the ionization partitions, while the two energy quantities together optimize the discrimination at low energy where the electron- and nuclear-recoil bands overlap. A BDT was trained for each detector using simulated background events (described below) and nuclear recoils from ^{252}Cf calibration weighted to mimic a WIMP energy spectrum, accounting for the selection criteria acceptance. The BDT discrimination thresholds for individual detectors were chosen simultaneously to minimize the expected 90% confidence level (C.L.) Poisson upper limit of the rate of passing events per WIMP exposure. The BDT was trained and optimized separately for 5, 7, 10, and $15 \text{ GeV}/c^2$ WIMPs. Events that pass any of the four WIMP-mass optimizations are accepted into the signal region as candidates. When a limit is set using the optimum interval method [30,31], this acceptance technique provides sensitivity to a range of masses but incurs only modest sensitivity loss compared to an analysis optimized at every WIMP mass. In addition to the BDT, two other discrimination methods were developed and similarly optimized for WIMP masses between 5 and $15 \text{ GeV}/c^2$. The BDT was chosen as the primary discrimination method before unblinding because of its better expected sensitivity on the background simulation data.

The acceptance of the preselection criteria and the BDT was evaluated using the fraction of ^{252}Cf nuclear recoils passing as a function of energy. Unlike WIMPs, the ^{252}Cf neutrons can multiply scatter within a single detector. To account for this effect, the measured acceptance of each detector is corrected upward, as a function of energy, by an $\sim 20\%$ relative shift. This correction is based on a GEANT4 [32] neutron simulation, which includes constraints on the resolution effects and the size of the fiducial volume. The uncertainty of the total acceptance is dominated by systematic uncertainty on the size of the fiducial volume and is shown in Fig. 1.

A background model was developed that includes Compton recoils from the gamma-ray background, 1.1–1.3-keV x rays and Auger electrons from L -shell electron-capture (EC) decay of ^{65}Zn , ^{68}Ga , ^{68}Ge , and ^{71}Ge , and decay products from ^{210}Pb contamination on the detectors and their copper housings. We normalize the flat Compton background to the observed rate of electron

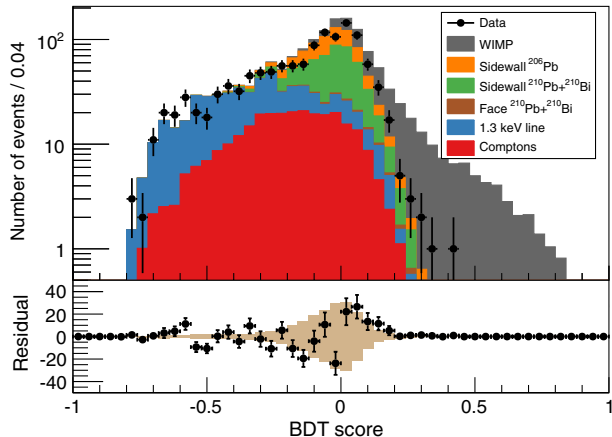


FIG. 2 (color online). Top: Stacked histogram showing the components of the background model passing the preselection criteria summed over all detectors (neutron backgrounds are negligible and not included). For comparison, a $10 \text{ GeV}/c^2$ WIMP with cross section $6 \times 10^{-42} \text{ cm}^2$ is shown on top of the total background. Events passing preselection criteria are overlaid (markers with statistical errors). A p -value statistic comparing the data to background model is 14% for this selection. Bottom: Difference between the data and the background expectation. Tan bars indicate the systematic uncertainty (68% C.L.) on the background estimate. Each component of the background model was computed prior to unblinding and was not fit or rescaled to match the data.

recoils in the range of $2.6\text{--}5.1 \text{ keV}_{\text{ee}}$. The average rate of the L -shell EC events is estimated by scaling the observed rate in the open data set by the ratio of the K -shell event rates in the WIMP-search and open data sets. We use GEANT4 to simulate the implantation and decay of ^{222}Rn daughters starting from ^{214}Po as described in Ref. [24]. Background components from ^{210}Pb decay products (betas, conversion electrons, and x rays), ^{210}Bi betas, and ^{206}Pb nuclei from ^{210}Po decays are considered, with rates normalized to the alpha and ^{206}Pb decay products of ^{210}Po under the assumption of secular equilibrium.

The background model is implemented using events from high-energy WIMP-search sidebands and calibration data as templates for low-energy backgrounds. Ionization and phonon pulses are scaled to lower energies, injected with noise from randomly triggered events throughout the data, and reconstructed as actual data. Templates for each background type were taken from different energy intervals ranging from 10 to 150 keV in recoil energy. ^{133}Ba calibration data and K -shell EC events are used as templates for the Compton recoils and L -shell EC events, respectively. Templates for ^{210}Pb daughters are sampled from high-energy betas and ^{206}Pb recoils.

Figure 2 shows the individual components of the background model as a function of the $10 \text{ GeV}/c^2$ BDT discrimination parameter after applying the preselection criteria. This background model was finalized prior to unblinding and predicted $6.1^{+1.1}_{-0.8}$ (stat + syst) events

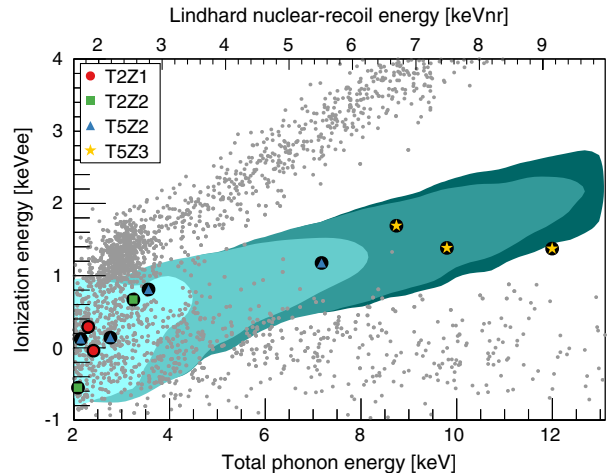


FIG. 3 (color online). Small gray dots are all veto-anticoincident single-scatter events within the ionization-partition fiducial volume that pass the data-quality selection criteria. Large encircled shapes are the 11 candidate events. Overlapping shaded regions (from light to dark) are the 95% confidence contours expected for 5, 7, 10, and $15 \text{ GeV}/c^2$ WIMPs, after application of all selection criteria. The three highest-energy events occur on detector T5Z3, which has a shorted ionization guard. The band of events above the expected signal contours corresponds to bulk electron recoils, including the 1.3-keV activation line at a total phonon energy of ~ 3 keV. High-radius events near the detector sidewalls form the wide band of events with near-zero ionization energy. For illustrative purposes, the Lindhard nuclear-recoil energy is provided as an approximate nuclear-recoil energy scale.

passing the BDT selection. Simulations of radiogenic and cosmogenic neutrons, as described in Ref. [22], predict an additional 0.098 ± 0.015 (stat) events. These estimates included only known systematic effects. Because the accuracy in background modeling required for a full likelihood analysis is difficult to achieve in a blind analysis of this type, the decision was made before unblinding to report an upper limit on the WIMP-nucleon cross section for this first analysis.

Upon unblinding, 11 candidates were observed, as indicated in Fig. 3. The events were found to be of high quality and occurring during good periods of experimental operation, except for the lowest-energy candidate, which has an abnormal pulse shape and is suspected to be noise. As seen in Table I, the observed number of events is consistent with the background prediction for most detectors. However, the three high-energy events in detector T5Z3 strongly disagree with the background prediction. The probability to observe at least this many background events on this detector is 4×10^{-4} . These events are observed on the only detector in this data set that has an ionization guard electrode shorted to ground. Although the background model was developed to account for the shorted channel, we realized after unblinding that the altered electric field may have affected the selection of the background model templates, potentially making the

TABLE I. Energies of candidate events in each detector labeled by tower (first number) and position within tower from top to bottom (second number). Expected background is based on the model used to train the BDT and includes the estimated systematic uncertainty. Differences in expected background across detectors reflect different trigger thresholds and background event rates. Event energies are calculated using the measured mean ionization energy for nuclear recoils.

Detector	Candidate energies (keV _{nr})	Expected background	Average 50% threshold (keV _{nr})
T1Z1	...	0.03 ^{+0.01} _{-0.01}	4.6
T2Z1	1.7, 1.8	1.4 ^{+0.2} _{-0.2}	1.5
T2Z2	1.9, 2.7	1.8 ^{+0.4} _{-0.3}	1.8
T4Z2	...	0.4 ^{+0.02} _{-0.02}	4.7
T4Z3	...	1.7 ^{+0.4} _{-0.3}	1.7
T5Z2	1.9, 2.3, 3.0, 5.8	1.1 ^{+0.3} _{-0.3}	2.0
T5Z3	7.0, 7.8, 9.4	0.13 ^{+0.06} _{-0.04}	1.7

background estimate on this detector inaccurate. We are currently pursuing follow-up simulations and sidewall event calibration of detectors with shorted ionization channels.

The background model is compared to unblinded events passing all preselection criteria in Fig. 2. The systematic uncertainty shown with tan fill is dominated by the uncertainty of the expected ionization of sidewall events originating from ^{210}Pb and ^{210}Bi . p -value statistics comparing the data passing the preselection criteria with the blind background model prediction range from 8% to 26% for the BDTs trained to each of the four WIMP masses. This reasonable compatibility based on the sum over all detectors suggests that the background model correctly reproduces most features of the observed background.

A 90% C.L. upper limit on the spin-independent WIMP-nucleon cross section was calculated using the optimum interval method without background subtraction. The calculation used standard halo assumptions as discussed in Ref. [33]. The result is shown in Fig. 4. Statistical and systematic uncertainties in the fiducial-volume efficiency, the nuclear-recoil energy scale, and the trigger efficiency were propagated into the limit by Monte Carlo simulation and are represented by the narrow gray band around the limit. The limit is consistent with the expected sensitivity for masses below 10 GeV/ c^2 as shown by the green band in Fig. 4. The discrepancy above 10 GeV/ c^2 is due to the three high-energy events in T5Z3, which are in tension with the background expectation.

This work represents the first search for WIMPs with the background rejection capability of the SuperCDMS detectors. The new iZIP sensor design has enabled more than an order of magnitude improvement in rejecting the dominant background observed at low energies in CDMS II, namely, events taking place on the faces and sidewalls of the

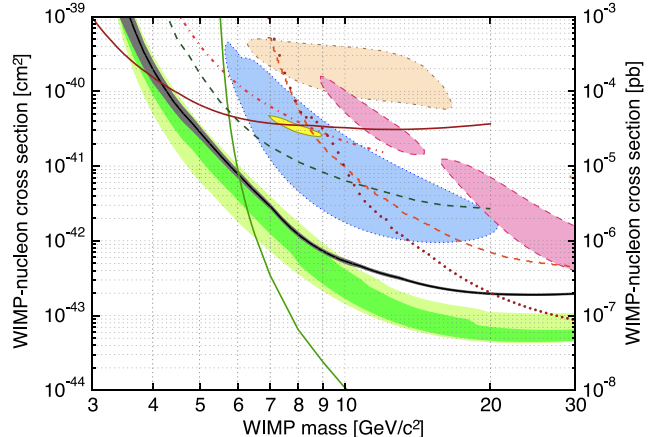


FIG. 4 (color online). The 90% confidence upper limit (solid black) based on all observed events is shown with 95% C.L. systematic uncertainty band (gray). The preunblinding expected sensitivity in the absence of a signal is shown as 68% (dark green) and 95% (light green) C.L. bands. The disagreement between the limit and sensitivity at high WIMP mass is due to the events in T5Z3, whose occurrence weakens the limit in this range. Closed contours shown are CDMS II Si [3] (dotted blue, 90% C.L.), CoGeNT [4] (yellow, 90% C.L.), CRESST-II [5] (dashed pink, 95% C.L.), and DAMA/LIBRA [34] (dash-dotted tan, 90% C.L.). The 90% C.L. exclusion limits shown are CDMS II Ge [22] (dotted dark red), CDMS II Ge low threshold [17] (dashed-dotted red), CDMSlite [20] (solid dark red, extending to ~ 3 GeV/ c^2), LUX [35] (solid green, extending to ~ 5.5 GeV/ c^2), XENON10 S2 only [19,36] (dashed dark green, extending to ~ 4.5 GeV/ c^2), and EDELWEISS low threshold [18] (dashed orange, extending to ~ 7 GeV/ c^2).

detectors. This analysis strongly disfavors a WIMP-nucleon scattering interpretation of the excess reported by CoGeNT. Because CoGeNT also uses a Ge target, interactions that depend on target material, such as isospin-violating interactions [37], cannot bring the two results into agreement. For standard spin-independent (SI) interactions, similar disagreement exists with WIMP interpretations of several other experiments, including CDMS II (Si); however, the different target nuclei ease the disagreement under different couplings within a broader effective field theory framework [38] and for different halo models [39]. For standard SI interactions, this measurement excludes new regions of WIMP-nucleon scattering for WIMP masses below 6 GeV/ c^2 , and for WIMP masses between 4 and 20 GeV/ c^2 it provides the most stringent limits for any target material other than xenon.

The SuperCDMS Collaboration gratefully acknowledges the contributions of numerous engineers and technicians. In addition, we gratefully acknowledge assistance from the staff of the Soudan Underground Laboratory and the Minnesota Department of Natural Resources. The iZIP detectors were fabricated in the Stanford Nanofabrication Facility, which is a member of the National

Nanofabrication Infrastructure Network. This work is supported in part by the National Science Foundation, by the United States Department of Energy, by NSERC Canada, and by MultiDark (Spanish MINECO). Fermilab is operated by the Fermi Research Alliance, LLC under Contract No. De-AC02-07CH11359. SLAC is operated under Contract No. DE-AC02-76SF00515 with the United States Department of Energy.

*Corresponding author.
adama@mit.edu

- [1] J. L. Feng, *Annu. Rev. Astron. Astrophys.* **48**, 495 (2010).
- [2] M. W. Goodman and E. Witten, *Phys. Rev. D* **31**, 3059 (1985).
- [3] R. Agnese *et al.* (CDMS Collaboration), *Phys. Rev. Lett.* **111**, 251301 (2013).
- [4] C. E. Aalseth *et al.* (CoGeNT Collaboration), *Phys. Rev. D* **88**, 012002 (2013).
- [5] G. Angloher *et al.*, *Eur. Phys. J. C* **72**, 1971 (2012).
- [6] R. Bernabei *et al.*, *Eur. Phys. J. C* **67**, 39 (2010).
- [7] D. Hooper and T. Linden, *Phys. Rev. D* **84**, 123005 (2011).
- [8] D. B. Kaplan, *Phys. Rev. Lett.* **68**, 741 (1992).
- [9] D. E. Kaplan, M. A. Luty, and K. M. Zurek, *Phys. Rev. D* **79**, 115016 (2009).
- [10] A. Falkowski, J. Ruderman, and T. Volansky, *J. High Energy Phys.* **05** (2011) 106.
- [11] R. R. Volkas and K. Petraki, *Int. J. Mod. Phys. A* **28**, 1330028 (2013).
- [12] K. M. Zurek, *Phys. Rep.* **537**, 91 (2014).
- [13] R. Essig, J. Kaplan, P. Schuster, and N. Toro, [arXiv:1004.0691](#).
- [14] C. Cheung, J. T. Ruderman, L.-T. Wang, and I. Yavin, *Phys. Rev. D* **80**, 035008 (2009).
- [15] D. Hooper and W. Xue, *Phys. Rev. Lett.* **110**, 041302 (2013).
- [16] D. S. Akerib *et al.* (CDMS Collaboration), *Phys. Rev. D* **82**, 122004 (2010).
- [17] Z. Ahmed *et al.* (CDMS Collaboration), *Phys. Rev. Lett.* **106**, 131302 (2011).
- [18] E. Armengaud *et al.* (EDELWEISS Collaboration), *Phys. Rev. D* **86**, 051701 (2012).
- [19] J. Angle *et al.* (XENON10 Collaboration), *Phys. Rev. Lett.* **107**, 051301 (2011).
- [20] R. Agnese *et al.* (SuperCDMS Collaboration), *Phys. Rev. Lett.* **112**, 041302 (2014).
- [21] W. Rau, *J. Phys. Conf. Ser.* **375**, 012005 (2012).
- [22] Z. Ahmed *et al.* (CDMS Collaboration), *Science* **327**, 1619 (2010).
- [23] D. Akerib *et al.* (CDMS Collaboration), *Phys. Rev. D* **72**, 052009 (2005).
- [24] R. Agnese *et al.* (SuperCDMS Collaboration), *Appl. Phys. Lett.* **103**, 164105 (2013).
- [25] B. Neganov and V. Trofimov, *Otkrytie. Izobreteniya* **146**, 215 (1985).
- [26] P. Luke, *J. Appl. Phys.* **64**, 6858 (1988).
- [27] J. Lindhard, V. Nielsen, M. Scharff, and P. Thomsen, *Integral Equations Governing Radiation Effects* (Munksgaard i kommunikation, Copenhagen, 1963).
- [28] J. Lewin and P. Smith, *Astropart. Phys.* **6**, 87 (1996).
- [29] A. Hoecker *et al.*, *Proc. Sci., ACAT* (**2007**) 040.
- [30] S. Yellin, *Phys. Rev. D* **66**, 032005 (2002).
- [31] S. Yellin, [arXiv:0709.2701](#).
- [32] S. Agostinelli *et al.* (Geant4 Collaboration), *Nucl. Instrum. Methods Phys. Res., Sect. A* **506**, 250 (2003).
- [33] Z. Ahmed *et al.* (CDMS Collaboration), *Phys. Rev. D* **83**, 112002 (2011).
- [34] C. Savage, G. Gelmini, P. Gondolo, and K. Freese, *J. Cosmol. Astropart. Phys.* **04** (2009) 010.
- [35] D. Akerib *et al.* (LUX Collaboration), *Phys. Rev. Lett.* **112**, 091303 (2014).
- [36] J. Angle *et al.* (XENON10 Collaboration), *Phys. Rev. Lett.* **110**, 249901(E) (2013).
- [37] J. L. Feng, J. Kumar, D. Marfatia, and D. Sanford, *Phys. Lett. B* **703**, 124 (2011).
- [38] A. L. Fitzpatrick, W. Haxton, E. Katz, N. Lubbers, and Y. Xu, [arXiv:1211.2818](#).
- [39] N. Anand, A. L. Fitzpatrick, and W. C. Haxton, [arXiv:1308.6288](#).